This is a preprint, the final version is subject to change, of the American Mineralogist (MSA)
Cite as Authors (Year) Title. American Mineralogist, in press.
(DOI will not work until issue is live.) DOI: http://dx.doi.org/10.2138/am.2013.4294

Revision 1

Elasticity of franklinite and trends for transition-metal oxide spinels

Hans J. Reichmann[1], Steven D. Jacobsen[2], Tiziana Boffa Ballaran[3]

[1]Helmholtz Centre Potsdam, German Research Centre for Geosciences GFZ, 14473 Potsdam, Germany
[2]Department of Earth and Planetary Sciences, Northwestern University, Evanston, IL 60208
[3]Bayerisches Geoinstitut, Universität Bayreuth, D-95440 Bayreuth, Germany

Abstract

The pressure dependence of single-crystal elastic moduli of a natural Mn-rich franklinite, $(Mn_{0.40}Fe^{2+}_{0.16}Zn_{0.37}Mg_{0.03})(Fe^{3+}_{1.94}Al_{0.08})O_4$, has been determined by GHz-ultrasonic interferometry in a diamond-anvil cell to 9.8 GPa. The room-pressure elastic constants of franklinite are C_{11} = 244(3) GPa, C_{12} = 142(4) GPa, and C_{44} = 77(2) GPa. Linear pressure derivatives of C_{11}, and C_{12} are 4.3(3) and 3.8(3), respectively, whereas the C_{44} modulus exhibits softening, fitted in the $P \leq 10$ GPa pressure range to $C_{44} = 77(2) + 0.29(2)P - 0.018(2)P^2$ GPa. The average of Hashin-Shtrikman bounds on the adiabatic bulk modulus (K_{S0}) of franklinite is 175(3) GPa, with pressure derivative $K_S' = 4.3(3)$, and the shear modulus G_0 = 66(2) GPa with G' = 0.09(3). The isothermal compressibility of franklinite was determined from a separate high-pressure, single-crystal X-ray diffraction experiment to 7.8 GPa, yielding K_{T0} = 173.5(7) GPa fitted with a fixed pressure derivative of $K_T' = 4$. When K' is fixed to the ultrasonic value of 4.3, we obtain K_{T0} = 172.2(7) GPa. In contrast to iron-free gahnite ($ZnAl_2O_4$), franklinite exhibits pressure-induced mode softening of C_{44} similar to magnetite (Fe_3O_4). Between end-member compositions $ZnFe_2O_4$ (franklinite) and $MnFe_2O_4$ (jacobsite) the bulk modulus decreases linearly with increasing %Mn, however we observe non-linear behavior in other elastic moduli, especially C_{44}, which displays a pronounced negative anomaly for the mid-range Mn composition. Applying Birch's law to AB_2O_4-type spinels reveals that oxide spinels containing transition metals on both A and B sites follow a distinct trend from other spinels.

Keywords: spinel, elasticity, transition metals, equation of state

1. Introduction

Spinel phases with generalized formula AB_2O_4 (8 formula units per unit cell, space group $Fd\bar{3}m$), are common non-silicate oxides in the crust and upper mantle. A special feature of this group is the ability to host a wide range of multi-valence transition metals. The compositional flexibility of spinels results in a multitude of natural and synthetic phases, many of which are used in magnetic, ferroelectric, semiconducting, and superconducting applications. MnZn-ferrites are among the most widely used soft ferrites in various types of transformers and magnetic recording heads (Sugimoto 1999). In petrological application, spinel solid solutions are recognized in marble and skarn deposits (Carvalho and Sclar 1988; Frondel and Baum 1974) and used in many geothermobarometers (e.g. Nichols et al. 1992). The $(Mg,Fe)_2SiO_4$ silicate spinel, ringwoodite, is likely a dominant phase in the lower-part of the mantle transition zone from 520-660 km depth.

Many spinels undergo phase transitions at elevated pressures (e.g. Fei et al. 1999; Funamori et al. 1998; Irifune et al. 2002; Levy et al. 2000) whereas other minerals with spinel structure do not exhibit a phase change to very high pressure. For example, gahnite ($ZnAl_2O_4$) does not exhibit a pressure-induced phase change up to 43 GPa (Levy et al. 2001). A closer look at the relation between phase transition and mineral composition reveals that spinels with two transition metals on the cation sites, like magnetite ($Fe^{2+}Fe^{3+}{}_2O_4$), tend to undergo the phase changes at a lower pressure than those with none or only one transition metal, such as spinel ($MgAl_2O_4$) and gahnite ($ZnAl_2O_4$).

Pressure-induced softening of shear-mode elastic moduli, such as C_{44}, is often associated with pressure-induced phase changes (e.g. Carpenter and Salje 1998). Magnetite undergoes a phase transition at 18-20 GPa (e.g. Dubrovinsky et al. 2003; Haavik et al. 2000; Pasternak et al. 1994) and exhibits a negative pressure dependence of C_{44} (Reichmann and Jacobsen 2004), whereas gahnite exhibits no phase transitions to 43 GPa (Levy et al. 2001)

and has a positive pressure dependence of C_{44} (Reichmann and Jacobsen 2006). In this paper we further study transition-metal oxide spinels and the high-pressure behavior of their elastic constants (C_{ij}), which reflect critical differences in interatomic bonding forces with varying composition and pressure.

Li and Fisher (1990) measured the elastic constants of single-crystal $ZnFe_2O_4$ at ambient conditions using the ultrasonic phase comparison method from 20-75 MHz. The elastic constants of $MnFe_2O_4$ under high magnetic field were measured with ultrasonic methods by Sakurai (1964). Li et al. (1991) determined the elastic constants of Co-ferrite spinels and summarized the elastic constants of end-member transition-metal spinels. To further characterize the elastic properties of MnZn-ferrite solid solutions, especially at high pressures, we have studied a natural franklinite single crystal of mid-range composition, $(Mn_{0.40}Fe^{2+}_{0.16}Zn_{0.37}Mg_{0.03})(Fe^{3+}_{1.94}Al_{0.08})O_4$, using GHz-ultrasonic interferometry in diamond-anvil cells. We measured the complete elastic tensor of franklinite to 9.8 GPa and report a non-linear pressure derivative of C_{44}, which approaches zero at above ~7 GPa. We also observe non-linear dependence of C_{44} on composition between Zn and Mn end-members. The isothermal compressibility of franklinite was also determined from separate single-crystal X-ray diffraction experiments. Finally, Birch's law is evaluated for spinels containing one or two transition metals on the *A* and *B* sites compared with other spinels.

2. Experimental

Sample characterization

Franklinite is an ordered normal spinel (Andreozzi et al. 2001; Pavese et al. 2000) and exhibits two transition metals (Zn and Fe) on the cation sites. The natural franklinite sample examined in this study originates from its type-locality in Franklin, New Jersey. Because of the crystal's octahedral form, it was possible to cut and polish sections parallel to (100) and (111) planes to within a few degrees. The basal plane of an octahedron represents the (100)

plane and the facets represent the (111) plane. We estimate the uncertainty in orientation of the polished sections is about ±2°. A (100) section was double-side polished to within a few arc-seconds of parallel and having a thickness of ~246 μm, measured using a micrometer, for room-pressure measurements of the P-wave velocity. For high-pressure experiments, (100) and (111) sections of the franklinite crystal were polished with an optical-quality finish together into thin section on the same slide to a thickness of ~45 μm, estimated by micrometer measurement. Electron microprobe analysis revealed spatial variations of the iron and zinc content. The Fe^{3+} content was determined by charge balance, and varies from 1.89 to 1.98 atoms per formula unit (apfu) and the Zn content varies from 0.35 to 0.41 apfu. The average composition over 10 measurement points of the sample is $(Mn_{0.40}Fe^{2+}_{0.16}Zn_{0.37}Mg_{0.03})(Fe^{3+}_{1.94}Al_{0.08})O_4$ (see **Table 1**). The density, $\rho = 5.038$ g/cm^3 was calculated using the measured lattice parameters and the stoichiometric composition determined from microprobe analysis

GHz-ultrasonic interferometry

The pressure-dependence of sound-wave velocities in franklinite were determined by GHz-ultrasonic interferometry in a diamond anvil cell (Jacobsen et al. 2002; Reichmann et al. 1998; Spetzler et al. 1993). In this technique, P-wave ultrasonic tone bursts are generated by thin-film ZnO transducers, coupled to the DAC through a single-crystal Al_2O_3 buffer rod, attached to the table face of one diamond anvil (Reichmann et al. 1998). To produce S-waves, a P-to-S conversion buffer rod made of yttrium-aluminum-garnet is attached to the table of the diamond anvil (Jacobsen et al. 2004). Using tone bursts of 20-100 ns, strain waves reflected at the front side overlap with reflections from the back side of the cylinder-shaped sample. Scanning the frequency between about 800 and 1200 MHz results in an interference pattern, from which the round trip travel time through the sample is determined analytically from the frequency spacing (Δf) between adjacent maxima and minima, corresponding to integer and half-integer acoustic wavelengths in the round-trip sample distance (e.g. Spetzler

et al. 1993). Longitudinal and transverse sound wave velocities $v_{P,S}$ are calculated using the equation

$$v_{P,S} = 2L/t \qquad \text{(eq. 1)}$$

where L is the sample thickness and t is the measured round-trip travel time.

To obtain transmission and quality acoustic reflections at GHz-frequencies where acoustic wavelengths at 1-GHz are in the order of 10 μm, the samples must be optically scratch-free with parallel front and back sides. The sample is placed on the diamond, which is coupled to the acoustic buffer rod with the transducer (Jacobsen et al. 2004; Reichmann et al. 1998). No bonding agent between diamond and sample was used. A 16:3:1 methanol - ethanol - water mixture was used as the pressure-transmitting medium, and a small amount of silica aerogel was included in the sample chamber to gently press the sample against the acoustic anvil for coupling and to prevent the alcohol mixture from flowing between the anvil and sample (Reichmann and Jacobsen 2004). The pressure in the sample chamber was determined before and after each run by the ruby fluorescence method (Mao et al. 1986).

X-ray Diffraction

A crystal plate polished parallel to (111) measuring 45 μm thick and 150 μm across was loaded into a BGI-designed diamond-anvil cell (Allan et al. 1996) with a culet size of 600 μm together with a ruby chip as the pressure calibrant (Mao at al. 1986). A 4:1 mixture of methanol : ethanol was used as pressure transmitting medium. A steel-plate (T301) gasket was employed between the anvils, pre-indented to 90-100 μm and drilled with a 280 μm sample chamber. The unit-cell parameters were determined at various pressures up to 7.8 GPa at ambient temperature on a Huber four-circle diffractometer (MoK_α radiation) using the 8-position centring procedure according to King and Finger (1979) and Angel et al. (2000). The centring procedure and vector least squares refinement of the unit cell constants were

134 performed using SINGLE04 (Angel and Finger 2011). Unit cell parameters at various
135 pressures are reported in **Table 2**.
136
137 **3 Results**
138 The unit-cell lattice parameter of the franklinite crystal measured at ambient
139 conditions is 8.4456(2) Å, compared to a = 8.4412(2) Å of synthetic ($ZnFe_2O_4$) spinel (Levy
140 et al. 2000) and a = 8.506(1) Å for $MnFe_2O_4$ (Butler and Buessem 1962). Compression data
141 from the single-crystal diffraction experiment are shown in **Figure 1a**. From analysis of the
142 normalized stress $F_E = P/[3f_E (1+2 f_E)^{5/2}]$ versus Eulerian strain $f_E = [(V_0/V)^{2/3}-1]/2$ plot (Angel
143 2000), it is clear that a 2nd order Birch–Murnaghan equation of state (BMII-EoS), i.e. with K'
144 fixed to the value of 4, is appropriate for fitting the P-V data (**Figure 1b**). The BMII-EoS
145 error-weighted fit resulted in an isothermal bulk modulus of K_{T0} = 173.5(7) GPa with a room
146 pressure volume V_0 = 602.41(4) Å^3, identical to that measured by single-crystal X-ray
147 diffraction, with V_0 = 602.40(4) Å^3 .The observation that the franklinite P-V data at $P \leq 10$
148 GPa can be described using a BMII-EoS, i.e. K' = 4 is in good agreement with the K' = 4.3(3)
149 obtained from the ultrasonic measurements (see next section). Fixing the value of K' to 4.3 we
150 obtain K_{T0} = 172.2(7) GPa and an identical value of V_0 = 602.41(4) Å^3. Considering that the
151 values of bulk moduli obtained from the two different fitting procedures coincident within
152 one standard deviation, the BMII-EoS values were used to calculate the length-changes on
153 compression during the ultrasonic experiments.
154 The elastic tensor (C_{ij}) of cubic minerals contains three independent moduli: C_{11}, C_{12}
155 and C_{44}. The elastic constants are related to the sound velocities by:

156 $$\rho(v_p^{[100]})^2 = C_{11} \qquad \text{(eq. 2)}$$

157 $$\rho(v_s^{[100]})^2 = C_{44} \qquad \text{(eq. 3)}$$

158 $$\rho(v_p^{[111]})^2 = (C_{11} + 4C_{44} + 2C_{12})/3 \qquad \text{(eq. 4)}$$

where ρ is the density and $v_{p,s}$ are longitudinal or transversal sound wave velocities in the [*uvw*] direction, denoted as superscript (e.g. Brugger 1965).

The room-pressure sample used to measure v_p in the [100] direction was 246 (±1) μm. The measured P-wave travel time at room-pressure was 70.65(2) ns, resulting in $v_p^{[100]}$ = 6960(30) m/s The thickness of samples used in the high-pressure diamond-anvil cell experiments was much less, about 45 μm, as determined by thickness measurements with a micrometer. Both (100) and (111) direction plates were polished together on the same slide. To determine the initial length (L_0) of the high-pressure samples, we measured the (100) thin section P-wave travel time and then calculated L_0 using equation (1) from the measured room-pressure velocity (**Table 3**). The calculated thickness L_0 of the high-pressure samples was 44.83(3) μm, in agreement with the micrometer measurement of 45(1) μm. The sample thickness L at high pressure was determined using the relation $(V/V_0)^{1/3} = (L/L_0)$, where V is the volume and V_0 is the volume at P=0. This relation holds for cubic (and isotropic) crystals. To determine the volume V at high pressure in the DAC, we utilized the isothermal equation of state determined in this study, with K_{T0}=173.5 GPa and fixed K' = 4. Knowing L_0 (44.83 μm), $V_0 = (L_0)^3$ and $V(P)$ from BMII-EoS, we calculated from the above equation $L(P)$.

In three separate experiments, the longitudinal and shear wave velocities of franklinite were determined in [100] and [111] directions as a function of pressure (**Table 3**). An S-wave acoustic interferogram and resulting sample travel times in franklinite at 9.8 GPa are shown in **Figure 2.** The room pressure values of elastic constants are C_{11} = 244(3) GPa, C_{12} = 142(4) GPa and C_{44} = 77(2) GPa. Variation of the elastic constants with pressure are shown in **Figure 3**. The pressure derivatives of C_{11} and C_{12} are linear over the measured pressure range of $P \leq 10$ GPa, with dC_{11}/dP = 4.3(3) and dC_{12}/dP = 3.8(3), shown by the solid lines in **Figure 3** representing linear fits to the data. Whereas, the C_{44} shear-mode sensitive modulus exhibits non-linear behavior indicative of mode softening, fitted to a polynomial equation at pressures $P \leq 10$ GPa with $C_{44} = 77(2) + 0.29(2)P - 0.018(2)P^2$ GPa.

The shear and adiabatic bulk moduli were calculated from the average of Hashin-Shtrikman bounds (Hashin and Shtrikman 1962; Hill 1952). Hashin and Shtrikman (1962) developed variational principles in elasticity to constrain aggregate moduli (K and G) of anisotropic media. In our study G_0 was found to be 66(2) GPa and K_{S0} = 175(3) GPa. Variation of the bulk and shear moduli of franklinite with pressure are shown in **Figure 4**. Due to the absence of any curvature in the bulk and shear moduli as a function of pressure, we fitted linear equations to the data with K' = 4.3(3) and G' = 0.09(3) (**Figure 4**). The aggregate sound velocities, which are calculated according to the equations

$$v_p = ((K+4/3\ G)/\rho)^{1/2} \quad \text{(eq. 5)}$$

$$v_s = (G/\rho)^{1/2} \quad \text{(eq. 6)}$$

vary with pressure according to the relations v_p = 7233(40) (m/s) + 38.3(1) P and v_s = 3630(25) (m/s) – 7.0(5) P.

4. Discussion

The natural franklinite sample in this study $(Mn_{0.40}Fe^{2+}_{0.16}Zn_{0.37}Mg_{0.03})(Fe^{3+}_{1.94}Al_{0.08})O_4$, represents a solid solution between ideal franklinite ($ZnFe_2O_4$) and jacobsite ($MnFe_2O_4$). Because the Mn-Zn ferrites are so widely used as soft ferrite cores in electronics (e.g. Sugimoto 1999), we first examine trends of elasticity along the Mn-Zn join.

The adiabatic bulk modulus of this natural franklinite (K_{S0} = 175 GPa) is about the average of bulk moduli for $ZnFe_2O_4$ (K_{S0} = 182.5 GPa) from Li and Fisher (1990) and $MnFe_2O_4$ (K_{S0} = 161 GPa) from Sakurai (1964), resulting in a variation of bulk modulus with Zn-Mn content that is approximately linear (**Figure 5**). The shear modulus of this natural franklinite (G = 66 GPa) lies 5% below the linear extrapolation between end-member compositions (**Figure 5**), but is not lower than pure $MnFe_2O_4$.

In contrast, individual elastic constants show non-linear compositional dependence, especially C_{44} (**Figure 5**). With increasing Mn-content relative to $ZnFe_2O_4$, the C_{11} elastic constant of the mid-range composition is about 8 GPa (~3%) above the linear extrapolation

between end members, whereas C_{12} is only 1% below the linear extrapolation between Zn and Mn end members. The C_{44} elastic constant for this mid-range composition falls about 14 GPa (16%) below the trend line extrapolated between end members, and furthermore exhibits a C_{44} = 77 GPa that is about 11% lower than the $MnFe_2O_4$ spinel with C_{44} = 86 GPa (Sakurai 1964). This trend implies that there is a minimum in C_{44} somewhere between $ZnFe_2O_4$ and $MnFe_2O_4$, possibly near this measured mid-range composition (**Figure 5**). A high-pressure modification of $ZnFe_2O_4$ was reported by Levy et al. (2000) above ~25 GPa, but on the basis of in-situ high-pressure powder X-ray diffraction a definitive structure could not be identified, although $CaTi_2O_4$ or $CaMn_2O_4$-type structures were determined to be the best candidates. Because of the minimum in C_{44} between $ZnFe_2O_4$ and $MnFe_2O_4$ we predict a similar phase transition to occur in natural franklinite but at lower pressures.

Compared with $ZnAl_2O_4$ (gahnite), which has K_{S0} = 209(5) GPa and G_0 = 104(3) GPa (Reichmann and Jacobsen 2006), the bulk and shear moduli of this mid-range franklinite are 17% and 36% lower. Whereas the elastic constants C_{11}, C_{12} of this franklinite are about 15% lower than $ZnAl_2O_4$, the C_{44} elastic constant is nearly 50% lower (**Table 4**). The pressure derivatives C_{11}' and C_{12}' of franklinite and gahnite are similar, however, C_{44}' of franklinite approaches zero above ~7 GPa, more similar to magnetite than gahnite (Reichmann and Jacobsen 2004). In **Figure 6**, the variation of C_{44} with pressure for franklinite, gahnite, magnetite, and spinel ($MgAl_2O_4$) are shown. The slopes of C_{44} of $MgAl_2O_4$ and $ZnAl_2O_4$ and of $ZnFe_2O_4$ and Fe_3O_4, respectively, are similar. The fact that dC_{44}/dP (franklinite) ≈ dC_{44}/dP (magnetite) < dC_{44}/dP (gahnite) is consistent with the observation that dC_{44}/dP decreases with increasing Fe- or transition metal content (Reichmann and Jacobsen 2006). A similar relationship of dC_{44}/dP with Fe-substitution was observed in the (Mg,Fe)O solid solution by Jacobsen et al. (2004), where compositions with less than ~50% Fe had positive dC_{44}/dP, mid-range compositions dC_{44}/dP ~0, and (Mg,Fe)O containing ~80% Fe and FeO show negative dC_{44}/dP.

In **Table 4**, we summarize the elastic properties of a wide compositional range of spinels. From **Table 4** it is apparent that the bulk moduli of spinels vary less with composition than does the shear modulus. In general, the shear modulus decreases with increasing transition metal occupancy of the A and B sites, with the exceptions of ringwoodite and chromite. Ringwoodite (γ-phase) is the only silicate spinel in our comparison. Chromite has a surprisingly high shear modulus considering that transition elements occupy both cation sites.

Liebermann (1970) showed that substituting Mg or Al in olivine and spinels with transition metals decreases v_p and v_s linearly. In **Figure 7**, the longitudinal and transversal sound wave velocities of various spinels from **Table 4** are plotted as a function of density. Both v_p and v_s decrease linearly with increasing density for spinels not containing transition metals, or only one transition metal on the A or B site (with the exception of Ni_2SiO_4). The solid line in **Figure 7** represents a linear fit to the v_p and v_s data for spinels hosting no or only one transition metal on the A or B site. The slopes are $dv_p/d\rho = -0.9$ (ms^{-1}/kgm^{-3}) and $dv_s/d\rho = -0.7$ (ms^{-1}/kgm^{-3}), respectively. Spinels with two transition metals on the A and B sites show a distinct deviation from this trend (with the exception of $FeCr_2O_4$). In **Figure 8** the bulk sound velocity $V_\Phi = (K/\rho)^{1/2}$ is plotted versus density, ρ. The bulk sound velocity decreases with higher density, which is in accordance with Birch's law (Birch 1952; Birch 1961) for isostructural minerals. However, it is also obvious that spinel structured minerals with two transition metals deviate from the general trend. The large deviation of spinels with two transition metals (on both A and B sites) from the linear trends in **Figure 7 and 8** suggest that non-ionic bonding forces begin to dominate elastic behaviour for those spinels.

The Cauchy relation, $0.5(C_{12} - C_{44}) = P$, is fulfilled when the solid exhibits Coulomb interaction between the ions. For stable ionic structures, the value of $0.5(C_{12} - C_{44})$ should be ~ 0 at room pressure. Spinels with the highest Cauchy number (i.e. those which violate the most this relation) are franklinite and magnetite (**Table 4**), a sign that covalent bonding increases at the expense of the Coulomb interaction when transition metals occupy both the

tetrahedral and octahedral sites. A peculiar feature of covalent bonding is the strong directional dependence compared to Coulomb interaction. This asymmetry in the bonding force may be one of the reasons for decreasing C_{44} of Fe-bearing spinel franklinite and magnetite as well as for the deviation from Birch's law (**Figure 8)**.

Another effect of the complex interatomic bonding forces for the Mn-Zn ferrites is depicted in **Figure 5**. The highly non linear decrease of the single crystal elastic moduli C_{ij} for the Mn-Zn ferrites with increasing Mn - content also suggest complex interatomic bonding forces with mixed valence transition metal spinels. Evaluating the bonding properties of transition metals is crucial to understand the elastic behavior of spinel-type structures with application to a wide range of problems both in geophysical and engineering sciences.

Acknowledgements

We thank Hubert Schulze, Kurt Klasinski, and Sven Linhardt at Bayerisches Geoinstitut for technical support. SDJ acknowledges support from the NSF EAR-0748707 (CAREER), the Carnegie/DOE Alliance Center (CDAC), and the David and Lucile Packard Foundation.

References

Allan, D.R., Miletich, R., and Angel, R.J. (1996) A diamond-anvil cell for single crystal X-Ray diffraction studies to pressures in excess of 10 GPa. Review of Scientific Instruments, 67, 840-842.

Andreozzi, G.B., Lucchesi, S., Skogby, H., and Della Giusta, A. (2001) Compositional dependence of cation distribution in some synthetic $(Mg,Zn)(Al,Fe^{3+})_2O_4$ spinels. European Journal of Mineralogy, 13, 391-402.

Angel, R.J. (2000) Equations of state. In R.M. Hazen and R.T. Downs, Eds. High-Temperature and High-Pressure Crystal Chemistry. Reviews im Mineraloy and Geochemistry. 41, 35-59.

Angel, R.J., Downs, R.T., and Finger, L.W. (2000) High-temperature high-pressure diffractometry. In R.M. Hazen and R.T. Downs, Eds. High-Temperature and High-Pressure Crystal Chemistry. Reviews in Mineralogy and Geochemistry, 41, 559-597.

Angel, R.J. and Finger, L.W. (2011) SINGLE: a program to control single-crystal diffractometers. Journal of Applied Crystallography, 44, 247-251.

Antao, S.M., Hassan, I., Crichton, W.A., and Parise, J.B. (2005) Effects of high pressure and high temperature on cation ordering in magnesioferrite, $MgFe_2O_4$, using in situ

synchrotron X-ray powder diffraction up to 1430 K and 6 GPa. American Mineralogist, 90, 1500-1505.

Bass, J.D., Weidner, D.J., Hamaya, N., Ozima, M., and Akimoto, S. (1984) Elasticity of the olivine and spinel polymorphs of Ni_2SiO_4. Physics and Chemistry of Minerals, 10, 261-272.

Birch, F. (1952) Elasticity and constitution of the Earth's interior. Journal of Geophysical Research, 57, 227.

Birch, F. (1961) The velocity of compressional waves in rocks to 10 kilobars. Journal of Geophysical Research, 66, 2199-2224.

Brugger, K.D. (1965) Pure modes for elastic waves in crystals. Journal of Applied Physics, 36, 759-768.

Butler, S.R. and Buessem, W.R. (1962) Variations of the lattice constant and line width of X-ray reflections from manganese ferrite. Journal of Physics and Chemistry of Solids, 23, 1661-1669.

Carpenter, M.A. and Salje, E.K.H. (1998) Elastic anomalies in minerals due to structural phase transitions. European Journal of Mineralogy, 10, 693-812.

Carvalho, A.V. and Sclar, C.B. (1988) Experimental determination of the $ZnFe_2O_4$- $ZnAl_2O_4$ miscibility gap with application to franklinite-gahnite exsolution intergrowths from the Sterling Hill zinc deposit, New Jersey. Economic Geology and the Bulletin of the Society of Economic Geologists, 83, 1447-1452.

Dubrovinsky, L.S., Dubrovinskaia, N.A., McCammon, C.A., Rozenberg, G.K., Ahuja, R., Osorio-Guillen, J.M., Dmitriev, V., Weber, H.P., Le Bihan, T., and Johansson, B. (2003) The structure of the metallic high-pressure Fe_3O_4 polymorph: experimental and theoretical study. Journal of Physics: Condensed Matter, 15, 7697-7706.

Fei, Y., Frost, D.J., Mao, H.-K., Prewitt, C.T., and Häusermann, D. (1999) In situ structure determination of the high-pressure phase of Fe_3O_4. American Mineralogist, 84, 203-206.

Frondel, C. and Baum, J.L. (1974) Structure and mineralogy of the Franklin zinc-iron-manganese deposit, New Jersey. Economic Geology and the Bulletin of the Society of Economic Geologists, 69, 157-180.

Funamori, N., Jeanloz, R., Nguyen, J.H., Kavner, A., and Caldwell, W. A. (1998) High-pressure transformations in $MgAl_2O_4$. Journal of Geophysical Research, 103(B9), 20813-20818.

Haavik, C., Stolen, S., Fjelllag, H., Hanfland, M., and Häusermann, D. (2000) Equation of state of magnetite and its high-pressure modification:Thermodynamics of the FeO-system at high pressure. American Mineralogist, 85, 514-523.

Hashin, Z. and Shtrikman, S. (1962) On some variational principles in anisotropic and nonhomogeneous elasticity. Journal of the Mechanics and Physics of Solids, 10, 335-342.

Hazen, R.M. (1993) Comparative Compressibilities of Silicate Spinels:Anomalous Behaviour of $(Mg,Fe)_2SiO_4$. Science, 259, 206-209.

Hearmon, R.F.S. (1984) The elastic constants of crystals and other anisotropic materials. In K.H.Hellwege, and A.M.Hellwege, Eds. Landolt-Börnstein Tables, III/18, p. 559. Springer Verlag, Berlin.

Hill, R. (1952) The elastic behaviour of a crstalline aggregate. Proceedings of the Physical Society of London A, 65, 349-354.

Irifune, T., Naka, H., Sanehira, T., Inoue, T., and Funakoshi, K. (2002) In situ X-ray observations of phase transitions in $MgAl_2O_4$ spinel to 40 GPa using multianvil apparatus with sintered diamond anvils. Physics and Chemistry of Minerals, 29, 645-654.

Jackson, J.M., Sinogeikin, S.V., and Bass, J.D. (2000) Sound velocities and elastic properties of γ-Mg_2SiO_4 to 873 K by Brillouin spectroscopy. American Mineralogist, 85, 296-303.

Jacobsen, S.D., Reichmann, H.J., Spetzler, H.A., Mackwell, S.J., Smyth, J.R., Angel, R.A., and McCammon, C.A. (2002) Structure and elasticity of single-crystal (Mg,Fe)O and a new method of generating shear waves for gigahertz ultrasonic interferometry. Journal of Geophysical Research, 107(B2), 2037.

Jacobsen, S.D., Spetzler, H.A., Reichmann, H.J. and Smyth, J.R. (2004) Shear waves in the diamond-anvil cell reveal pressure - induced instability in (Mg,Fe)O. Proceedings of the National Academy of Science, 101, 5967-5871.

King, H.E. and Finger, L.W. (1979) Diffracted beam crystal centring and its application to high-pressure crystallography. Journal of Applied Crystallography, 12, 374-378.

Levy, D., Diella, V., Pavese, A., Dapiaggi, M., and Sani, A. (2005) *P-V* equation of State, thermal expansion, and *P-T* stability of synthetic ($ZnCr_2O_4$ spinel). American Mineralogist, 90(7), 1157-1162.

Levy, D., Pavese, A., and Hanfland, M. (2000) Phase transition of synthetic zinc ferrite spinel ($ZnFe_2O_4$) at high pressure, from synchrotron X-ray powder diffraction. Physics and Chemistry of Minerals, 27, 638-644.

Levy, D., Pavese, A., Sani, A., and Pischedda, V. (2001) Structure and compressibility of synthetic $ZnAl_2O_4$ (gahnite) under high-pressure conditions from synchrotron X-ray powder diffraction. Physics and Chemistry of Minerals, 28, 612-618.

Li, Z. and Fisher, E.S. (1990) Single crystal elastic constants of zinc ferrite ($ZnFe_2O_4$). Journal of Material Science Letters, 9, 759-760.

Li, Z., Fisher, E.S., Liu, J.Z., and Nevitt, M.V. (1991) Single crystal elastic constants of Co-Al and Co-Fe spinels. Journal of Material Science, 26, 2621-2624.

Liebermann, R.C. (1970) Velocity-density systematics for the olivine and spinel phases of Mg_2SiO_4 - Fe_2SiO_4. Journal of Geophysical Research, 75(20), 4029-4034.

Mao, H.K., Xu, J., and Bell., P.M. (1986) Calibration of the ruby pressure gauge to 800 Kbar under quasi hydrostatic conditions. Journal of Geophysical Research, 91(B5), 4673-4676.

Nichols, G.T., Berry, R.F., and Green, D.H. (1992) Internally consistent gahnitic spinel - cordierite-garnet equilibria in the FMASHZn system: geothermobarometry and applications. Contributions to Mineralogy and Petrology, 111, 362-377.

Pasternak, M.P., Nasu, S., Wada, K., and Endo, S. (1994) High-pressure phase of magnetite. Physical Review B, 50, 6446-6449.

Pavese, A., Levy, D., and Hoser, A. (2000) Cation distribution in zinc ferrite ($Zn_{0.97}$ $Fe_{2.02}$ O_4) from in situ high-temperature neutron diffraction. American Mineralogist, 85, 1497-1502.

Reichmann, H.J., Angel, R.A., Spetzler, H.A., and Bassett, W.A. (1998) Ultrasonic interferometry and X-ray measurements on MgO in a diamond anvil cell. American Mineralogist, 83, 1357-1360.

Reichmann, H.J. and Jacobsen, S.D. (2004) High-pressure elasticity of a natural magnetite crystal. American Mineralogist, 89, 1061-1066.

Reichmann, H.J. and Jacobsen, S.D. (2006) Sound wave velocities and elastic constants of $ZnAl_2O_4$ spinel and implications for spinel-elasticity systematics. American Mineralogist, 91, 1049-1054.

Sakurai, J. (1964) Ultrasonic propagation in nickel and Mn-ferrite at high magnetic fields. Journal of the Physical Society of Japan, 19(3), 311-317.

Sinogeikin, S.V., Bass, J.D., and Katsura, T. (2003) Single-crystal elasticity of ringwoodite to high pressures and high temperatures: implications for 520km seismic discontinuity. Physics of the Earth and Planetary Interiors, 136, 41-66.

Spetzler, H.A., Chen, G., Whitehead, S., and Getting, I.C. (1993) A new ultrasonic interferomter for the determination of equation of state parameters of sub-millimeter single crystals. Pure and Applied Geophysics, 141, 341-377.

Sugimoto, M. (1999) The past, present, and future of ferrites. Journal of the American Ceramic Society, 82, 269-280.

Wang, H. and Simmons, G. (1972) Elasticity of some mantle crystal structures 1. Pleonaste and hercynite spinel. Journal of Geophysical Research, 77, 4379 -4392.

Yoneda, A. (1990) Pressure derivatives of elastic constants of single crystal MgO and $MgAl_2O_4$. Journal of Physics of the Earth, 38, 19-55.

Figure Captions

Figure 1. (A) Variation of the unit-cell volume of franklinite with pressure (this study), normalized to the room-pressure experimental volume (V_0). The solid line represents a BMII-EoS fit to the data. The EoS curves of magnetite (Reichmann and Jacobsen 2004, dotted line) and $ZnAl_2O_4$ (Reichmann and Jacobsen 2006, dashed line) are also shown for comparison. (B) Normalized pressure F_E versus Eulerian strain f_E for franklinite compression, where $f_E = ((V_0/V)^{2/3} - 1)/2$ and $F_E = P/(3f_E(1+2f_E)^{5/2})$

Figure 2. (A) S-wave acoustic interferogram measured at 9.8 GPa by interfering the diamond-culet echo with the sample echo (solid line). The dashed line shows variation of the diamond-culet echo with frequency, used to remove system interference in the demodulated spectrum, shown in (B). The travel time (C) is determined from the frequency spacing (Δf) between maxima and minima for the best fit of m, the number of integer acoustic wavelengths in the round-trip distance for the first frequency maximum. In (C), the result of choosing adjacent values of m is shown.

Figure 3. Variation of the elastic tensor C_{ij} of franklinite with pressure.

Figure 4. Variation of the shear modulus G and adiabatic bulk modulus K_S of franklinite with pressure. The shear modulus is invariant with pressure within the uncertainty of the measurements.

Figure 5. Trends of various elastic moduli with composition between end-members $ZnFe_2O_4$ (Li and Fisher 1990) and $MnFe_2O_4$ (Sakurai 1964). The dashed lines are linear extrapolations between the two end-member points. The mid-range franklinite (this study) shows linear trends with composition for the bulk modulus and C_{12} elastic modulus, whereas other elastic moduli display non-linear behavior. C_{44} of the mid-range franklinite (this study) is lower than either end-member, suggesting that there is an intermediate composition with minimum C_{44}.

Figure 6. Comparison of C_{44} between franklinite (this study), magnetite (Reichmann and Jacobsen 2004), gahnite (Reichmann and Jacobsen 2006), and spinel (Yoneda 1990). Minerals with transition elements on their tetrahedral and octahedral sites (franklinite and magnetite) exhibit invariant or slightly negative C_{44} dependence with pressure.

Figure 7. The compressional (circles) and longitudinal (squares) sound wave velocities of spinels as a function of density (Birch's law). References are given in Table 4. Spinels containing transition metals on both the A and B sites deviate from the trend of spinels containing no transition metals, or only transition metals on the A or B sites.

Figure 8. The bulk sound velocity $V_\Phi=(K/\rho)^{1/2}$ versus density ρ. According to Birch's law V_Φ decreases (linearly) with increasing ρ for isostructural minerals. Spinels with two transition metals deviate significantly from the trend of those spinels with one or no transition metals.

452

453 **Table 1** Weight percent oxides from ten different microprobe analysis spots on the franklinite

454 sample.

455

Measurement	1	2	3	4	5	6	7	8	9	10
Oxide										
MgO	0.60	0.73	0.77	0.56	0.63	0.69	0.74	0.84	0.84	0.88
Al_2O_3	1.75	0.95	1.03	1.95	1.74	1.51	1.16	0.79	0.90	0.44
SiO_2	0.04	0.01	0.01	0.01	0.00	0.00	0.01	0.00	0.00	0.00
CaO	0.00	0.00	0.00	0.00	0.00	0.01	0.02	0.00	0.01	0.02
TiO_2	0.18	0.12	0.10	0.10	0.17	0.16	0.12	0.10	0.12	0.07
Cr_2O_3	0.00	0.00	0.02	0.02	0.01	0.01	0.00	0.00	0.01	0.00
MnO	12.34	10.69	10.60	13	12.52	12.15	11.34	10.45	10.66	9.72
FeO	67.85	75.92	74.91	64.96	68.06	68.86	71.36	77.12	75.52	80.62
ZnO	13.34	6.42	8.18	14.60	12.91	12.06	10.65	6.70	6.70	3.60
Total (%)	**96.09**	**94.84**	**95.62**	**95.33**	**96.03**	**95.44**	**95.39**	**96.02**	**94.40**	**95.36**

456
457

458

459

460

461 **Table 2.** Compression data for franklinite from single-crystal X-ray diffraction. Uncertainties
462 are given in parentheses.

P (GPa)*	*a* (Å)	*V* (Å^3)
0.0001	8.4456 (2)	602.40 (4)
0.04	8.4446 (2)	602.19 (5)
1.68	8.4178 (2)	596.48 (5)
2.11	8.4122 (2)	595.28 (5)
2.47	8.4070 (3)	594.18 (6)
3.66	8.3894 (2)	590.47 (5)
4.43	8.3783 (2)	588.12 (5)
5.40	8.3638 (3)	585.07 (5)
6.54	8.3472 (3)	581.60 (6)
7.34	8.3354 (3)	579.13 (6)
7.36	8.3350 (2)	579.05 (5)
7.78	8.3306 (2)	578.12 (5)
3.15[§]	8.3975 (3)	592.18 (6)

463
464 *Uncertainty in pressure is 0.05 GPa.
465 [§]Measured on decompression
466

3. High-pressure sound velocity and elastic moduli data for Mn-franklinite.

$P^{\S}$ (GPa)	$\rho^{\S\S}$ (kg/m^3)	$v_p^{[100]}$ (km/s)	C_{11} (GPa)	K_S* (GPa)	G* (GPa)	P (GPa)	ρ (kg/m^3)	$v_p^{[111]}$ (km/s)	C_{12} (GPa)	P (GPa)	ρ (kg/m^3)	$v_s^{[100]}$ (km/s)	C_{44} (GPa)
0.0001	5038	6.96(3)	244(3)	175(3)	66(2)	0.0001	5038	7.44†	142(4)	0.0001	5038	3.92†	77(2)
0.72	5059	6.98(3)	247(3)	178(3)	66(2)	2.97	5122	7.56(3)	154(4)	1.5	5081	3.91(1)	78(2)
1.25	5074	7.01(3)	249(3)	180(3)	66(2)	4.34	5160	7.60(3)	159(4)	2.1	5098	3.91(1)	78(2)
1.96	5094	7.03(3)	252(3)	183(3)	66(2)	4.71	5170	7.62(3)	161(4)	2.6	5112	3.91(1)	78(2)
3.62	5140	7.12(3)	261(3)	190(3)	67(2)	5.05	5179	7.63(3)	162(4)	4.2	5156	3.90(1)	78(2)
5.23	5183	7.16(3)	266(3)	197(3)	66(2)	5.75	5197	7.66(3)	166(4)	4.8	5172	3.89(1)	78(2)
5.55	5192	7.18(3)	268(3)	198(3)	66(2)	6.40	5215	7.68(3)	168(4)	5.4	5188	3.89(1)	78(2)
5.72	5197	7.18(3)	268(3)	199(3)	66(2)	6.66	5221	7.68(3)	169(4)	6.4	5215	3.88(1)	79(2)
6.43	5215	7.22(3)	272(3)	203(3)	66(4)	6.78	5225	7.69(3)	170(4)	7.1	5233	3.87(1)	79(2)
7.38	5240	7.25(3)	276(3)	207(3)	66(2)	7.09	5232	7.71(3)	172(4)	7.8	5251	3.87(1)	79(2
						7.31	5238	7.72(3)	173(3)	8.3	5264	3.86(1)	79(2)
										8.5	5269	3.86(1)	78(2)
										8.9	5279	3.86(1)	78(2)
										9.1	5284	3.86(1)	79(2)
										9.5	5294	3.85(1)	79(2)
										9.8	5302	3.85(1)	79(2)

§ The uncertainty in pressure is estimated to be 0.05 (GPa)
§§ The uncertainties in densities are estimated to be 10(kg/m^3)
* Calculated at pressures corresponding to C_{11} measurements using values of C_{12} and C_{44} from fits.
† $v_p^{[111]}$ and $v_s^{[100]}$ at P = 0.0001(GPa) determined from extrapolation of high pressure data.

476 **Table 4.** Elastic properties of spinel-structured minerals.

Formula (mineral name)	Ref.*	Method† P_{max}	ρ_0 (kg/m^3)	C_{11} (GPa) C_{11}' C_{11}'' (GPa^{-1})	C_{12} (GPa) C_{12}' C_{12}'' (GPa^{-1})	C_{44} (GPa) C_{44}' C_{44}'' (GPa^{-1})	$[(2C_{44}+C_{12})/C_{11}-1]$	Cauchy Relation $(C_{12}-C_{44})/2$	K_S (GPa) K_S' K_S'' (GPa^{-1})	K_t (GPa) K_t'	G (GPa) G'	v_P (m/s) dv_P/dP (ms^{-1}/GPa)	v_S (m/s) dv_S/dP (ms^{-1}/GPa)
$MgAl_2O_4$ (spinel)	(1)	MHz 6 GPa	3578	282.9 5.59 -0.65	155.4 5.69 -0.64	154.8 1.44 -0.19	0.644	0.3	197.9 5.66 -0.65		110.0 0.61		
γ-$(Mg_{0.91}Fe_{0.09})_2SiO_4$ (ringwoodite)	(2)	BS 16 GPa	3701	329(2) 6.2(2)	118(3) 2.8(3)	130(2) 0.8(2)	0.149(17)	-6.0	188(3) 4.1(3)		120(2) 1.3(2)	9690(20)	5680(10)
$FeAl_2O_4$ (hercynite)	(3)	MHz 0 GPa	4280	266.0	182.5	133.5	0.690	24.5	210.3		84.5	8677	4428
$(Mn_{0.40}Fe^{2+}_{0.16}Zn_{0.37}Mg_{0.03})(Fe^{3+}_{1.94}Al_{0.08})O_4$ **(franklinite)**	**This study**	**GHz 10 GPa**	**5038**	**244(3) 4.3 (3)**	**142(4) 3.8 (3)**	**77(2) 0.29(2) -0.018(2)**	**0.21(25)**	**31**	**175(3) 4. 3(3)**	**173.5(7) 4 (fixed)**	**66(2) 0.09(3)**	**7233(40) 38.3(1)**	**3630(25) -7.0(5)**
$(Zn_{0.74}Fe_{0.18}Mg_{0.08})Al_2O_4$ (gahnite)	(4)	GHz 9 GPa	4464	290(3) 4.48(10)	169(4) 5.0(8)	146(2) 1.47(3)	0.590(25)	11.5	209(5) 4.8(3)		104(3) 0.5(2)	8830(40) 47.2(5)	4824(40) 0.68(7)
$ZnAl_2O_4$ (gahnite)	(5)	XRD 43 GPa	4597							201.7(9) 7.62(9)			
γ-Fe_2SiO_4	(6)	XRD 5 GPa	4845							207(3) 4.8 (fixed)	104.9		
$FeCr_2O_4$ (chromite)	(7)		5090	322	144	117	0.174	13.5	203.3		104.9		
$FeFe_2O_4$ (magnetite)	(8)	GHz 9 GPa	5196	260.5(1.0) 5.14(13)	148.3(3.0) 5.39(10)	63.3(1.5) -0.13(4)	0.055(17)	42.5	185.7(3.0) 5.1(1)	180.0(1.0) 5.2(4)	60.3(3.0) −0.1(1)	7157(30) 47.4(4)	3407(20) −12.5(3)
$ZnFe_2O_4$ (franklinite)	(9)	XRD 37 GPa	5319							166(3) 9.3(6)			
γ-Ni_2SiO_4	(6)	XRD 5 GPa	5339							233(2) 4.8 (fixed)			
$ZnCr_2O_4$ (zincochromite)	(10)	XRD 21 GPa	5366							183(4) 7.9(6)			
$MgFe_2O_4$ (magnesioferrite)	(11)	MHz 0.3GPa	4554							165.6(6)	76.2(2)	7698(11)	4111(5)
Ni_2SiO_4	(12)	BS	5351	366(3)	155(3)	106(1)	0.0027	24.5	226		106	8275	4447
γ-Mg_2SiO_4	(13)	BS	3559	327(3)	114(2)	131(2)	0.149	-8.5	185(3)		120(2)	9850(60)	5820(30)
$CoAl_2O_4$	(14)	MHz 0 GPa	4416	290.5	170.3	138.6	0.540	15.8	210.4		99.1	8807	4738
$CoFe_2O_4$	(14)	Ultrasonic 0 GPa	5304	257.1	150.0	85.3	0.247	32.3	185.7		70.8	7267	3653
$MnFe_2O_4$	(15)	Ultrasonic 0 GPa	5000	213	135	86	0.441	24.5	161		62.6	6993	3539

477
478 *(1) (Yoneda 1990); (2) (Sinogeikin et al. 2003); (3) (Wang and Simmons 1972); (4) (Reichmann and Jacobsen 2006); (5) (Levy et al. 2001); (6) (Hazen 1993); (7) (Hearmon 1984); (8) (Reichmann
479 and Jacobsen 2004); (9) (Levy et al. 2000); (10) (Levy et al. 2005); (11) (Antao et al. 2005); (12) (Bass et al. 1984); (13) (Jackson et al. 2000); (14) (Li et al. 1991); (15) (Sakurai 1964).
480 † MHz = MHz-ultrasonic interferometry; GHz = GHz-ultrasonic interferometry; BS = Brillouin scattering; XRD = X-ray diffraction (static compression).

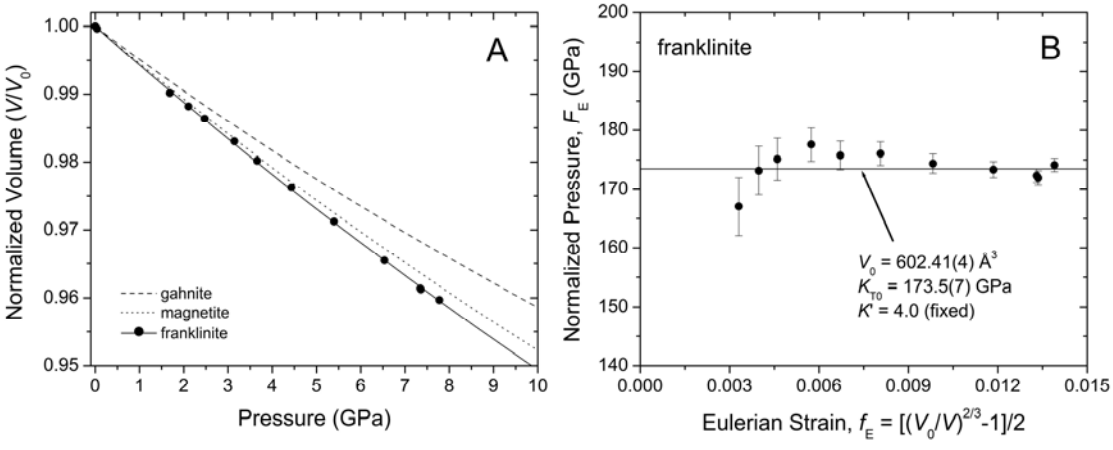

481

482

483 **Figure 1.**

484

485

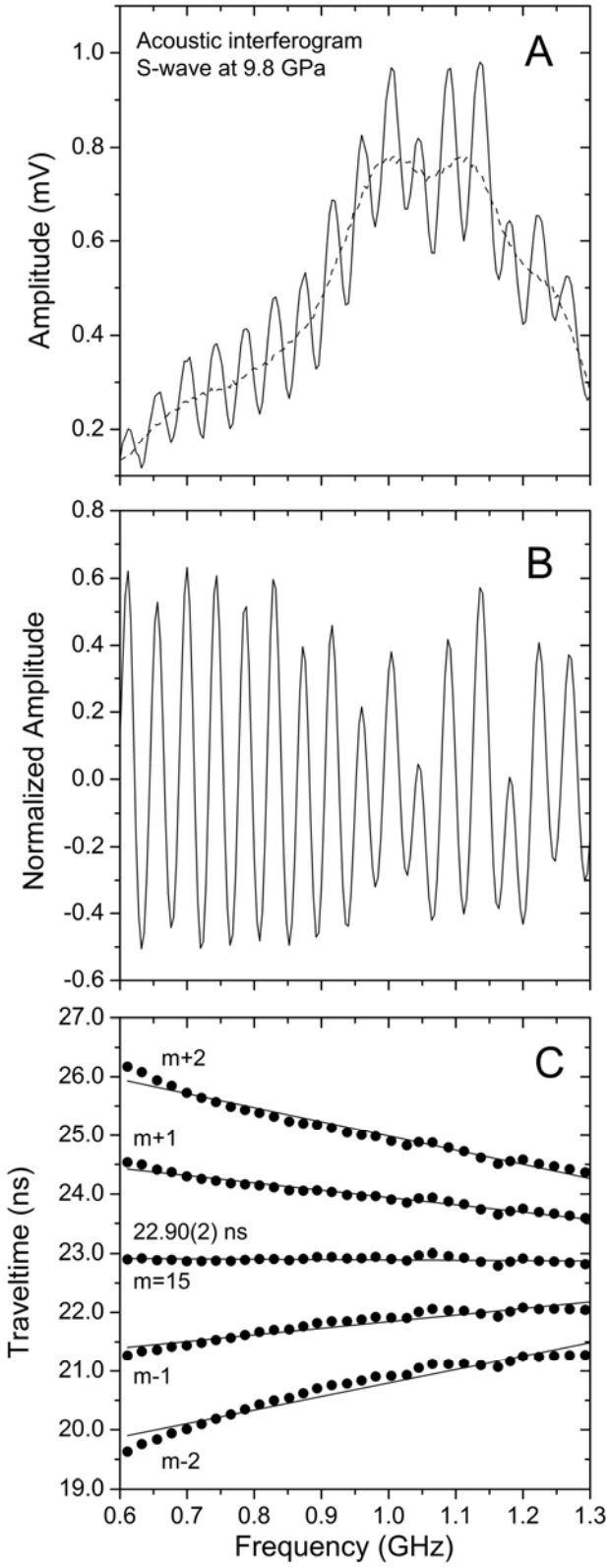

Figure 2.

490

491

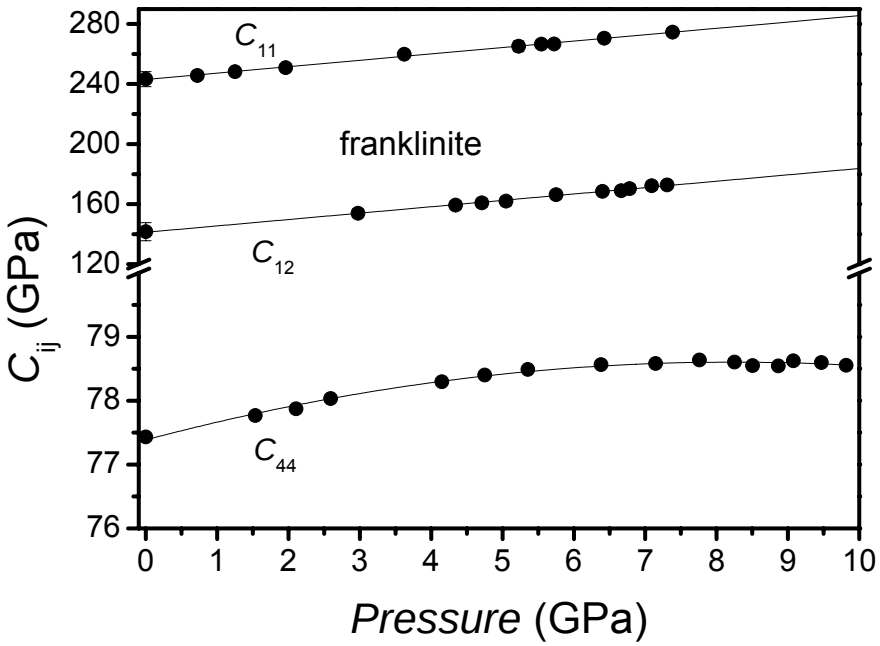

492

493 **Figure 3.**

494

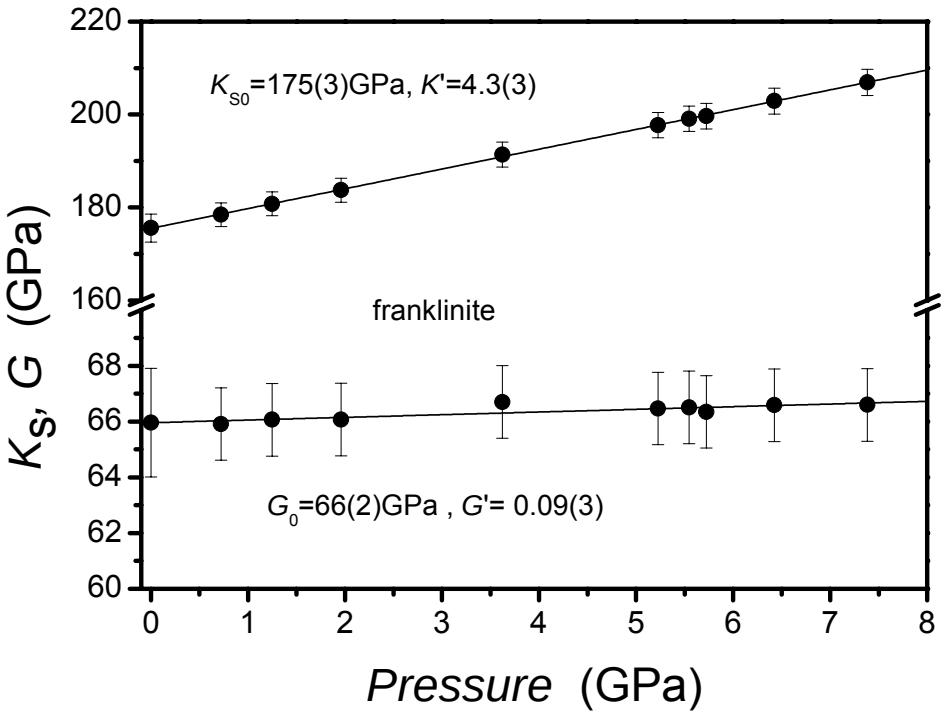

Figure 4.

499

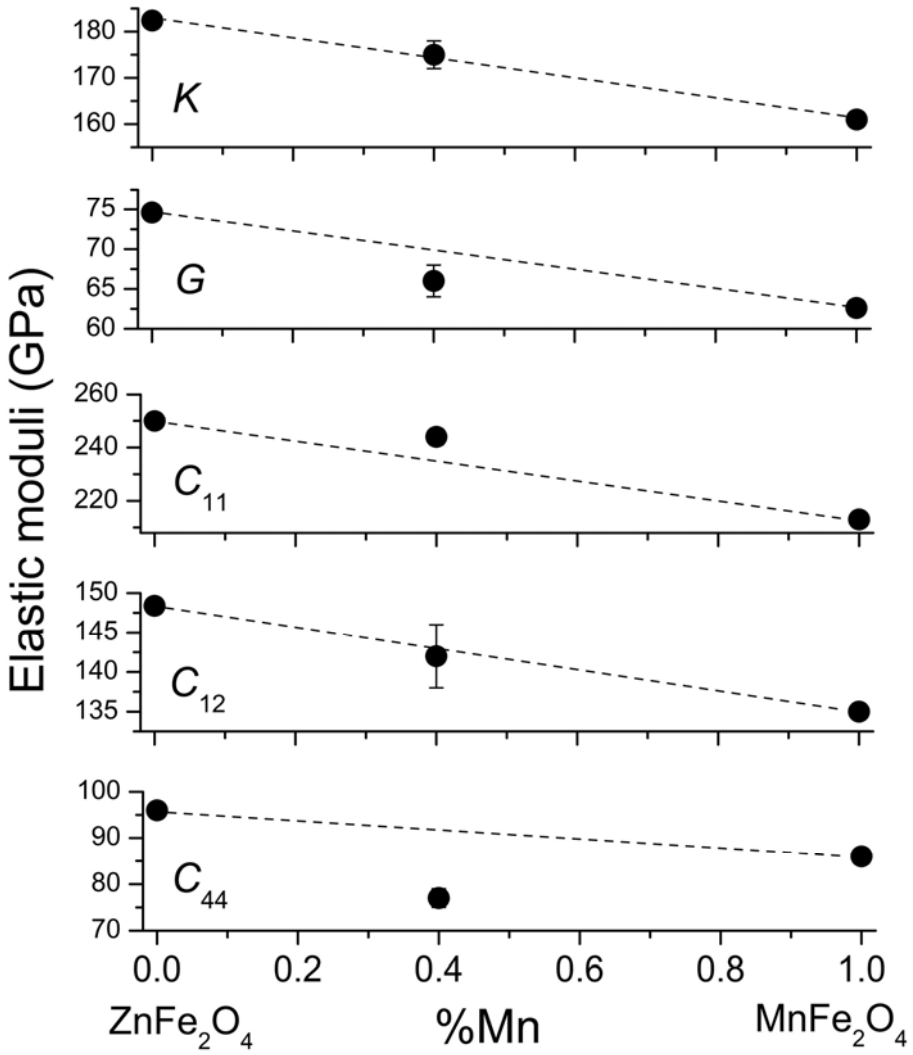

500

501

502 **Figure 5.**

503

504

505

506

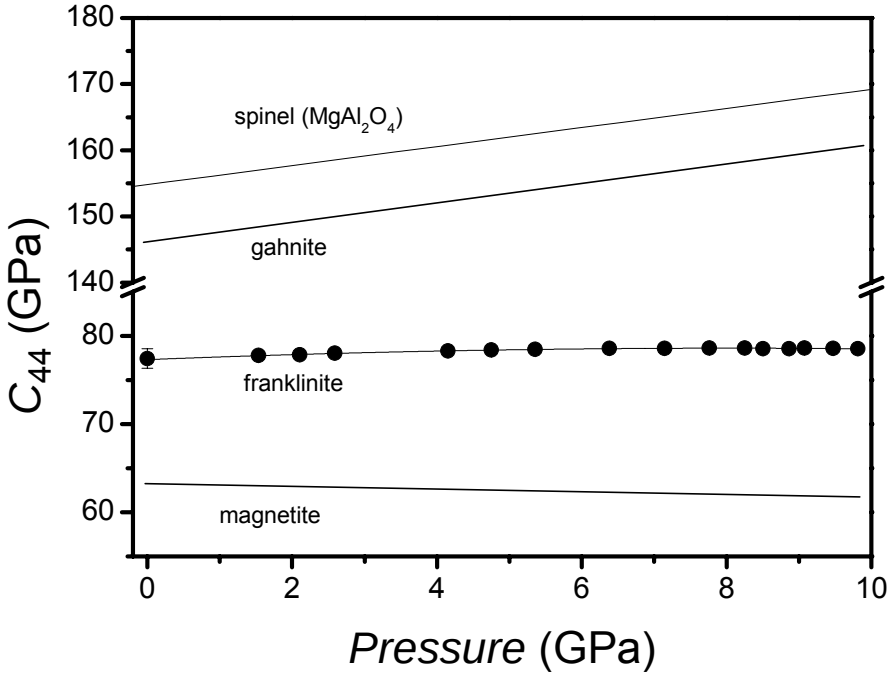

507

508

509 **Figure 6.**

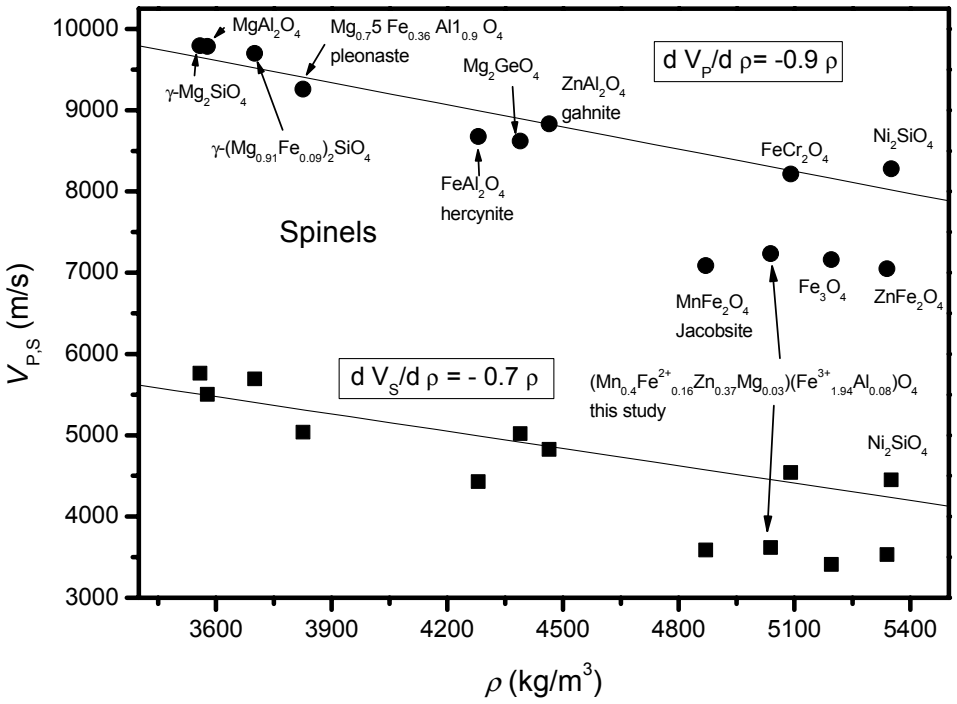

Figure 7.

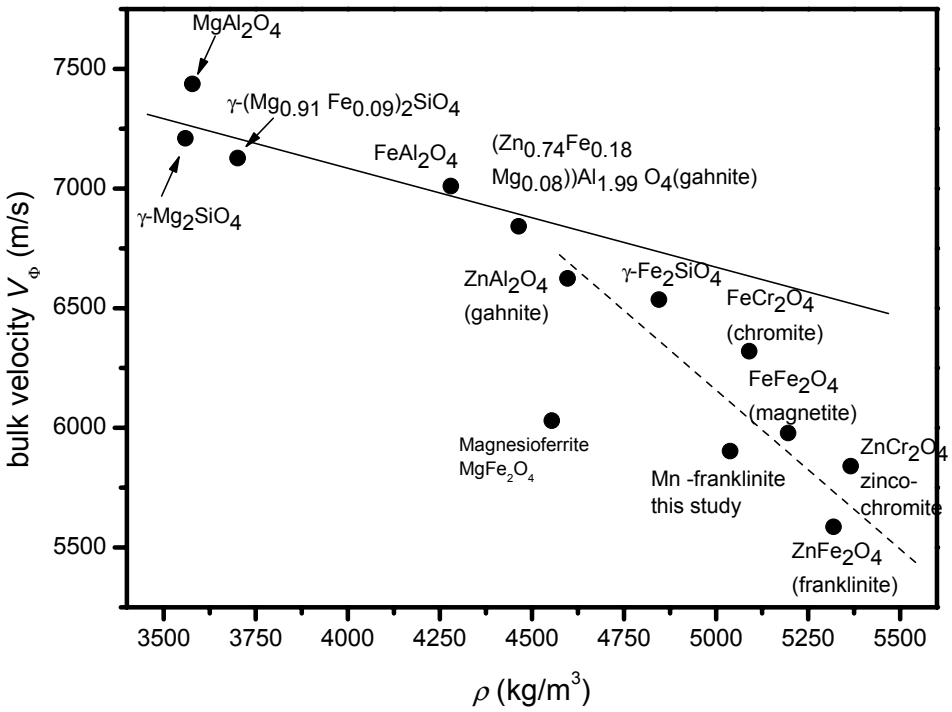

Figure 8.